Probing the mineralized tissue-adhesive interface for tensile nature and bond strength

*Rizacan Sarikaya[a,b], Qiang Ye[b], Linyong Song[b], Candan Tamerler[b,c], Paulette Spencer[b,c] and Anil Misra[b,c,d]**

[a] Department of Mechanical and Aerospace Engineering, Trine University, 1 University Ave, Angola, IN, 46703, USA
[b]Institute for Bioengineering Research (IBER), University of Kansas, 1530 W. 15th St, Lawrence, KS 66045, USA
[c]Department of Mechanical Engineering, University of Kansas, 1530 W. 15th St, Lawrence, KS 66045, USA
[d]Civil, Environmental and Architectural Engineering Department, University of Kansas, 1530 W. 15th St, Lawrence, KS 66045, USA

***Corresponding author:** Dr. Anil Misra **Email:** amisra@ku.edu

Manuscript submitted for publication to:
Journal of the Mechanical Behavior of Biomedical Materials

ABSTRACT

The mechanical performance of the dentin-adhesive interface contributes significantly to the failure of dental composite restorations. Rational material design can lead to enhanced mechanical performance, but this requires accurate characterization of the mechanical behavior at the dentin-adhesive interface. The mechanical performance of the interface is typically characterized using bond strength tests, such as the micro-tensile test. These tests are plagued by multiple limitations including large variations in the test results. The challenges associated with conventional tensile tests limit our ability to unravel the complex relationships that affect mechanical behavior at the dentin-adhesive interface. This study used the diametral compression test to overcome the challenges inherent in conventional bond strength tests. The bovine femur cortical bone tissue was considered as a surrogate material (the mineralized tissue) for human dentin. Two different adhesive formulations, which differed by means of their self-strengthening properties, were studied. The tensile behavior of the mineralized tissue, the adhesive polymer, and the bond strength of the mineralized tissue – adhesive interface was determined using the diametral compression test. The diametral compression test improved the repeatability for both the tensile and bond strength tests. The rate dependent mechanical behavior was observed for both single material and interfacial material systems. The tensile strength and bond strength of the mineralized tissue-adhesive interface was greater for the self-strengthening formulation as compared to the control.

Keywords: Bond Strength, Dental Adhesives, Mineralized Tissue, Biomaterials, Diametral Compression Test, Indirect Tensile Test, Interface

1. Introduction

Comprehensive understanding of the bond mechanics at the dentin – adhesive interface is critical to address dental caries, a major health problem: It was estimated that 3.5 billion cases related to dental caries were reported worldwide in 2017 [1-8]. Unhealthy teeth are frequently repaired using resin-based composites [9, 10]. The treatment aims to regain the natural appearance and load bearing capacity of the tooth. This particular treatment (i.e., dental composite restoration) provides relief to patients. However, the relief may be limited to 5 to 7 years [11]. Material design that is informed by a comprehensive understanding of the factors leading to failure offers promise for extending the lifetime of composite restorations.

The overall clinical performance of the dental composite restoration is determined, in part, by the contribution of each component at the dentin-adhesive interface [12-14]. The composition of the interface includes dentin, adhesive polymer, and the hybrid layer. The hybrid layer is demineralized dentin collagen partially or completely infiltrated by adhesive polymer. The mechanical performance of the interface depends on the load bearing characteristics of the materials that make up the dentin – adhesive interface.

Bond strength is the typical property that demonstrates the load bearing capacity of the dentin-adhesive interface. A variety of loading modes and applications are used for bond strength tests, including tensile, micro tensile, shear, micro shear, pull- and push-out tests [15-22]. Interfacial imperfections, substrate characteristics, adhesive polymer, hybrid layer, specimen geometry, specimen size, and loading configuration are the factors that significantly affect bond strength [23].

Micro tensile and shear tests achieve relatively reliable characterization of bond strength when performed over a small interfacial cross-sectional area (i.e., approximately 1 mm^2) [21, 22, 24]. Cohesive type of failure is prevented in micro tests as the cross-sectional area is small compared

to macro-scale applications [25]. However, large variations are reported for micro tensile and shear bond strength testing modes. For example, broad variations were observed in micro tensile (i.e., 6 to 75 MPa) and micro shear modes (i.e., 6 to 39 MPa) [26, 27]. Large variations, particularly in conventional tensile testing, can be related to its underlying mechanics. Particularly, this type of mechanical testing presents inherent challenges in terms of sample preparation and consistent application of boundary conditions. The boundary conditions often diverge from the application of relatively pure tensile loading and uniform distribution of stress.

The diametral compression test constitutes an efficient alternative that overcomes many of the abovementioned challenges. Diametral compression test is also known as split tensile test and indirect tensile test [28] and is commonly used for tensile strength measurements on single material systems and composites [28-34]. Recent studies have used the diametral compression test for bond strength measurement on interfacial specimens, such as post-dentin disks and bovine dentin-adhesive-composite [34-36]. The typical test configuration is based on a specimen with a disk geometry. The disk is compressed on its curved edges between two load platens [28]. This load application induces tensile action that is perpendicular to the axis of loading [31]. Notably, the diametral compression test allows a convenient specimen preparation and load application compared to the conventional tensile test. The geometry is simplified to a disk and the load is applied without any attachment, fixation or grips. The disk specimen is simply placed between load platens. In this study, the diametral compression test was modified to improve the repeatability of the experiments by introducing a hole in the disk center [37]. This central hole constitutes a preset weakness in heterogeneously defective materials, such as the mineralized tissue. The preset weakness stimulates the initiation of diametral failure.

The performance of the interfacial material system is determined by the behavior of each component, i.e. the dentin, adhesive polymer, and, more importantly the hybrid layer. Therefore, the tensile nature of the involved components requires particular attention during the investigation of the bond strength at the dentin-adhesive interface. Due to its inherent weakness [38-42], the hybrid layer dictates the bond strength at the dentin-adhesive interface.

This study considered the bovine femur cortical bone as a surrogate material for human dentin. Cortical bone possesses microstructural and compositional similarities with dentin. These similarities include relatively comparable organic to volume ratio and complementary composition, i.e., calcium phosphate based apatite, type-I collagen and fluid [43]. Besides these similarities, the bovine femur has greater accessibility for specimen preparation compared to the human tooth.

The complete nature of the mineralized tissue – adhesive interface was investigated in this study. Using the diametral compression test, these investigations focused on two aspects. The first aspect concentrated on exploring the tensile damage and failure of each component of the mineralized tissue – adhesive interface. For this aspect, a modified diametral compression test was performed on the mineralized tissue and the adhesive polymer. The second aspect was the interfacial characterization via the diametral compression test to characterize the bond strength at the mineralized tissue – adhesive interface. Both single material and interfacial diametral compression tests were conducted at different loading rates, as illustrated in Fig. 1. Different loading rates were selected to reveal the rate-dependent nature of these material systems. In addition, we note that teeth in function are subjected to a range of loading rates during chewing/biting. Moreover, recent studies led to the development of new polymer chemistries for dental adhesives. These new polymer chemistries significantly improve the mechanical

performance of adhesive polymer by introducing photoacid-induced sol-gel reaction [44-47]. To this end, two adhesive formulations, i.e., with and without γ-methacryloxypropyl trimethoxysilane (MPS), were evaluated using both single material and interfacial mechanical tests. MPS was reported to provide self-strengthening property to dental adhesives leading to superior strength [48].

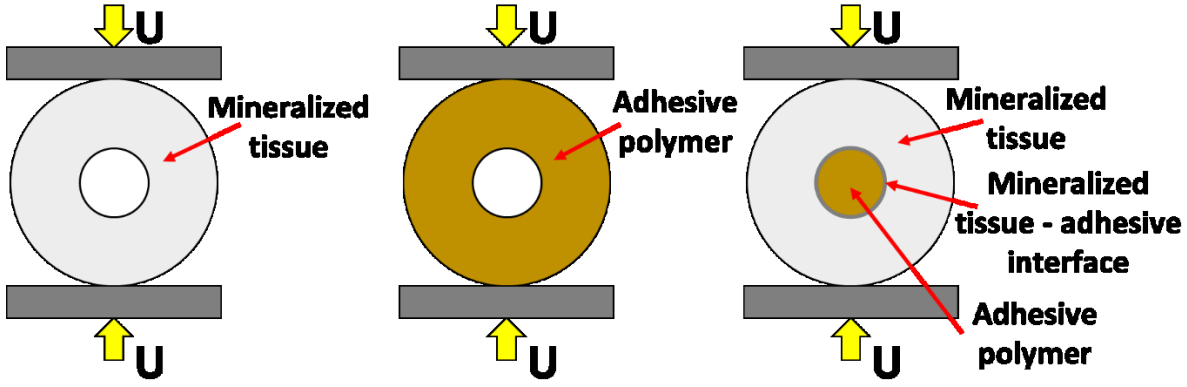

Fig. 1. The representation of the diametral compression test of disk specimens made of the mineralized tissue and adhesive polymer and the interfacial specimen made of the mineralized tissue and adhesive to perform bond strength measurement.

2. Materials and Methods

2.1 Sample Preparation

The experimental characterization was done on two types of specimens. The first type is the ring specimen, where a disk geometry has a hole in the center. The second type is the interfacial specimen, where the ring specimen has an adhesive inclusion in the hole. The specimens were derived from the mineralized tissue and adhesive resins.

2.1.1 Mineralized Tissue

The mineralized tissue specimens were obtained from a bovine femur's cortical bone (Fig. 2(a)) [37]. Initially, the bovine femur was coarsely cut into large sections. Afterwards, the sections along the diaphysis of the bone were cut into smaller sections via a diamond saw (Isomet 1000, Buehler, Lake Bluff, IL). The diametral compression test specimens were shaped using a mini lathe (Mini lathe G8688, Grizzly, Bellingham, WA). The machining processes were conducted while keeping the specimens hydrated. The geometry of each specimen was a 1.5 mm-thick disk with a diameter of 3 mm and a 1mm-diameter hole. The hole was placed using a drill bit mounted in the mini lathe. The given dimensions were achieved with a tolerance of +/- 0.05 mm. In total, 30 specimens were prepared from the cortical bone. From the prepared bone specimens, 10 were used as ring specimens and 20 were used for preparing interfacial specimens. All of the disks were stored in phosphate-buffered saline solution with a pH of 7.4 (Sigma-Aldrich, St. Louis, MO) and ~0.1 wt% sodium azide [49].

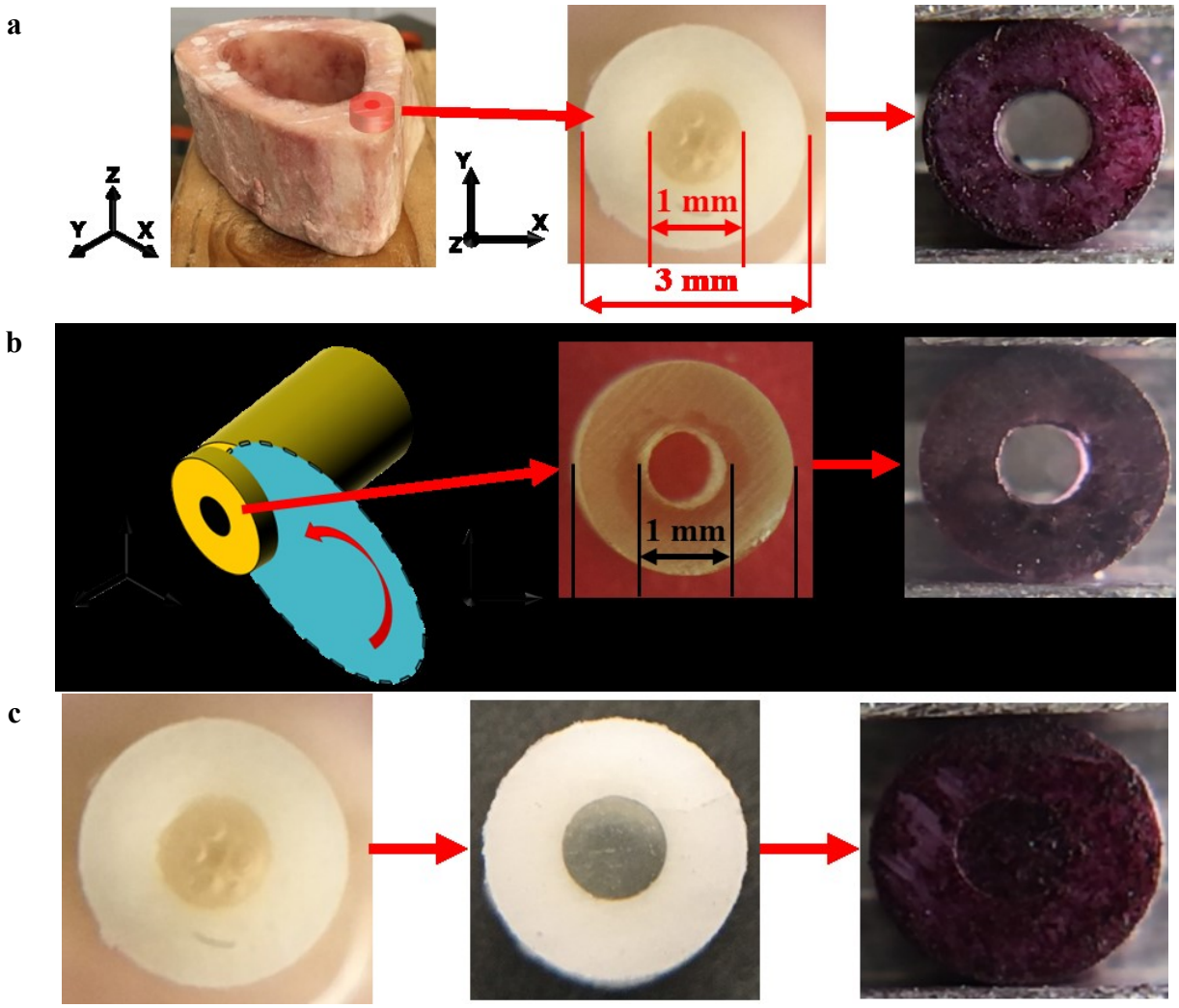

Fig. 2. (a) Bovine cortical bone tissue (mineralized tissue) ring specimen derived from the diaphysis of the bone. (b) Adhesive polymer specimen that was cut into a disk specimen from a larger adhesive polymer cylinder that contains a hole in its center. (c) The bovine cortical bone ring specimen that is applied with the adhesive resin in the center hole in order to prepare an interfacial specimen. All specimens were dyed with a black permanent marker before the mechanical test to reveal the fracture path. After machining, all specimens have a diameter of 3 mm, a thickness of 1.5 mm and a hole diameter of 1 mm.

2.1.2 Adhesive Polymers

The adhesive polymers were prepared according to the following protocol. Initially, 2,2-Bis[4-(2-hydroxy-3-methacryloxypropoxy) phenyl]propane (BisGMA), 2-hydroxyethyl methacrylate (HEMA), camphoroquinone (CQ), ethyl-4-(dimethylamino) benzoate (EDMAB), and diphenyliodonium hexafluorophosphate (DPIHP) were purchased from Sigma-Aldrich (St. Louis, MO). γ-methacryloxypropyl trimethoxysilane (MPS) was obtained from MP Biomedicals (Solon, OH). Moreover, methacryloxyethoxytrimethylsilane (MES, 95%) was obtained from Gelest Inc. (Morrisville, PA). All chemicals were used as received without further purification. Fig. A1 presents the chemical structures of components that were used in the formulations (see the Appendix).

The control and experimental adhesive formulations, C1 and E1, respectively, were prepared by making the neat methacrylate-based resins (see the Appendix, Table A1). In detail, 58 wt% HEMA, 30 wt% BisGMA, and 10 wt% MES (C1) or MPS (E1) were mixed and CQ (0.5 wt%), EDMAB(0.5 wt%), and DPIHP (1.0 wt%) were used as the three component photoinitiator (PIs) system [50-52]. The monomer/PIs mixtures were prepared in brown glass vials under amber light [46].

To achieve the desired geometry for the diametral compression test, the adhesive polymer specimens were initially prepared as cylindrical samples. The prepared resin (~400 μL) was injected into a Celprogen clear 96-well microplates (CAT#E36110-37-96well), covered with mylar film, and photo-polymerized with a commercial visible-light-curing unit (Spectrum®800, Dentsply, Milford, DE) at 550 mW/cm^2 for 40 s. The polymerized cylindrical samples (~6.4 mm diameter and 11 mm height) were stored in the dark at 37 °C for 5 days before further processing. Following the same approach as the sample preparation of the mineralized tissue, adhesive

polymer specimens were shaped using the mini lathe, the specimens were kept hydrated during the machining process. The adhesive polymer specimens were prepared with the same geometry and dimensions as the cortical bone disk specimens (Fig. 2(b)). In total, 6 specimens were prepared from each formulation. Since the adhesive polymers are being developed for application in the wet, oral environment, it is important to understand the behavior in wet conditions and thus, all adhesive specimens were kept in distilled, deionized water for 5 days [48, 53]. The polymer specimens became swollen in water and their final dimensions were measured. For E1 adhesive specimens, the thickness was ~1.60 mm, the diameter was ~3.10 mm and the hole diameter was ~0.84 mm. For C1 adhesive specimens, the thickness was ~1.61 mm, the diameter was ~3.16 mm and the hole diameter was ~1.00 mm.

2.1.3 Interfacial Specimens

The interfacial specimens were prepared using 20 mineralized tissue ring specimens and the adhesive resins, E1 and C1. We particularly focus upon wet bonding to etched mineralized tissue via hybrid layer formed as collagen-adhesive composites [54].” The interfacial specimen was designed as a disk geometry of two concentric parts. The mineralized tissue ring specimens were used for the outer layer and the center inclusions were created by applying each E1 and C1 adhesive formulations separately (Fig. 2(c)). The mineralized tissue disk specimens were divided into two groups, where each adhesive formulation was applied to 10 disk specimens. In order to apply the adhesives, the hole surface in the mineralized tissue disk was first etched with a mixture of phosphoric acid and ethanol (60% v/v 35% H3PO4+ 40% v/v ethanol) for 10 min and then rinsed with deionized water. The resin was applied to fill the hole in the mineralized tissue disk and light-irradiated for 40 s at 23±2 °C using a commercial light source (Spectrum® 800, Dentsply,

Milford, DE. Light intensity is 550 mW/cm^2). Finally, the mineralized tissue - adhesive interfacial specimens were stored in 1x PBS solution (containing ~0.1 wt% sodium azide) at 37°C for 5 days, to allow time for dark-cure. In the oral environment, the mineralized tissue – adhesive interface is exposed to wet conditions. Therefore, the wet conditions were maintained to obtain clinically relevant measurements.

2.2 Mechanical Test

The mechanical test was conducted via Microtest stage (Microtest 200N Stage, Deben UK Ltd., Bury St Edmunds, UK) (Load cell range: 200N with the accuracy 1% of full scale range, extension range: 10 mm with the position readout accuracy of 0.1% of full scale range, standard speed range: 0.1 mm/min to 1.5 mm/min) (Fig. 3). Two sets of specimens were tested and two different loading rates were applied on each set. The loading rates were selected as the high loading rate of 1 mm/min and the low loading rate of 0.2 mm/min. The number of ring specimen for C1 and E1 formulations was chosen to be 3, respectively, for each test-type (loading-rates) given the repeatability of the polymerized adhesives. For the mineralized tissue and interfacial specimen, considering their heterogeneity, the number of specimen was chosen to be 5 for each test-type (loading-rates). All specimens were kept hydrated during the mechanical experiments. The specimens were only removed from the wet environment to perform the mechanical tests. The test was video recorded via in-house slow-motion microscopy, 1280x720 pixels and 240 frames per second.

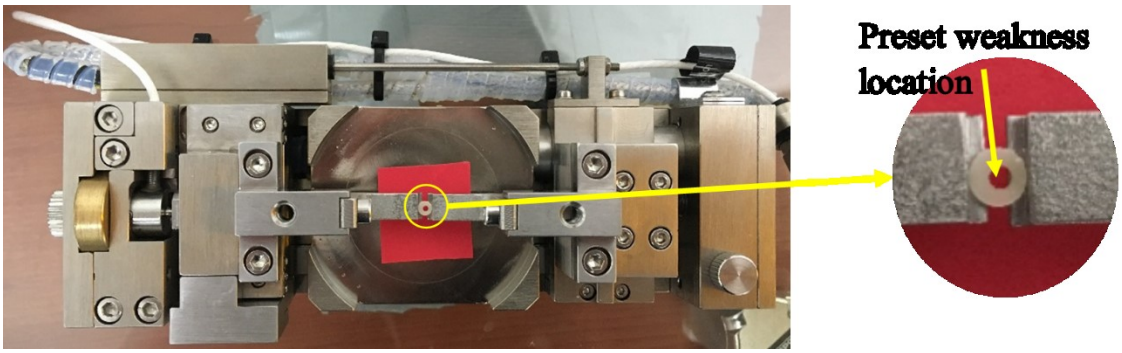

Fig. 3. Micro-tensile test stage where the diametral compression test was performed and the close-up image of a ring specimen. The hole in the center constitutes a preset weakness location to promote failure.

3. Results

Mechanical tests provided the force-displacement relationships regarding the tensile nature of the mineralized tissue and polymer adhesives, C1 and E1. Moreover, the bond strength information was obtained from the testing of the interfacial specimens of the mineralized tissue – C1 adhesive and the mineralized tissue – E1 adhesive. Additionally, deformation and failure patterns were obtained from the video recordings.

3.1 Mineralized Tissue

From the bovine cortical bone specimens that were subject to 1 mm/min loading rate, the average peak force was 77.61 N where the minimum peak force was 69.49 N and the maximum force was 84.11 N (Fig. 4(a)(Row 1)). The average failure displacement was 0.39 mm where the minimum failure displacement was 0.37 mm and the maximum failure displacement was 0.44 mm (see the Appendix, Table A2).

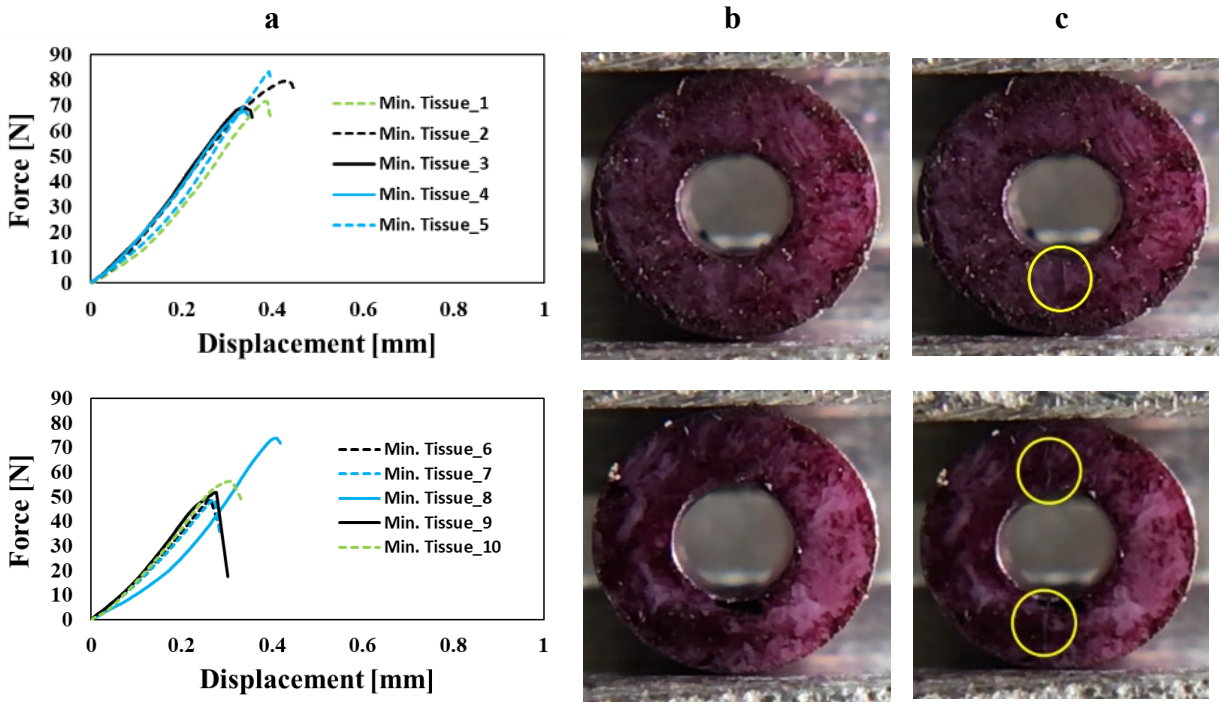

Fig. 4. (a) Force-displacement results obtained from the diametral compression test of the mineralized tissue ring specimens. Snapshots from the diametral compression test: (b) the undeformed specimen and (c) the specimen after failure (post-failure). Row 1: at 1 mm/min loading rate. Row 2: at 0.2 mm/min loading rate.

As noted from the comparison of Fig. 4(b)(Row 1) with Fig. 4(c)(Row 1), the image after failure reveals that a discoloration zone emerged on the surface of the mineralized tissue specimen (circled with yellow line) at 1 mm/min loading rate. This discoloration indicates where the fracture initiated and how it propagated. The fracture started inside out along the loading axis and propagated towards the loading surface. The quality of the image was compromised due to a water film on the specimen surface. The specimens need to be hydrated to prevent changes in the microstructure due to dehydration. We note that the water film also pose difficulty for optical imaging techniques. In the future, we will improve the mechanism of keeping the specimen

hydrated and image acquisition such that they can potentially be analyzed via digital image correlation or other advanced image analysis techniques to obtain field measurements.

For the mineralized tissue ring specimens subjected to 0.2 mm/min loading rate, the average peak force yielded 51.50 N where the minimum peak force was 48.9 N and the maximum force was 56.44 N ignoring the one outlier (Fig. 4(a)(Row 2)). Besides, the failure displacement was averaged as 0.28 mm where the minimum was 0.27 mm and the maximum was 0.31 mm. It is observed that both the average peak force and the average failure displacement of the mineralized tissue ring specimens at 0.2 mm/min loading rate were lower than their average peak force and displacement at 1 mm/min loading rate, respectively (see the Appendix, Table A2).

When the mineralized tissue ring specimen was subject to the loading rate of 0.2 mm/min, the discoloration zone was observed at the same location as noted with the 1 mm/min loading rate. The failed specimen (Fig. 4(c)(Row 2)) had the fracture initiation around the hole and along the loading axis. This is clearly observed when the failed specimen's surface is compared to the intact specimen (Fig. 4(b)(Row 2)). The fracture path was circled with a yellow line and it was found to be between the load surface and the hole on the loading axis. The observed fracture initiation location and the fracture path of the mineralized tissue at loading rate of 0.2 mm/min matched with the location of initiation and evolution of its fracture at 1 mm/min loading rate.

3.2 Adhesive Polymers

The polymer ring specimens made of C1 formulation and tested at 1 mm/min had an average peak force of 28.50 N (Fig. 5(a)(Row 1)). The minimum peak force was measured 27.57 N and the maximum was 29.74 N. The average displacement at failure was 0.52 mm where the minimum and maximum were 0.46 mm and 0.57 mm, respectively. The average failure force of C1 adhesive specimens at 1 mm/min loading rate was substantially smaller than the average failure force of the

mineralized tissue at both 1 mm/min and 0.2 mm/min loading rate. On the other hand, C1 adhesive specimens failed at a larger displacement at 1 mm/min loading rate compared to the mineralized tissue specimens at both 1 mm/min and 0.2 mm/min loading rates (see the Appendix, Table A2).

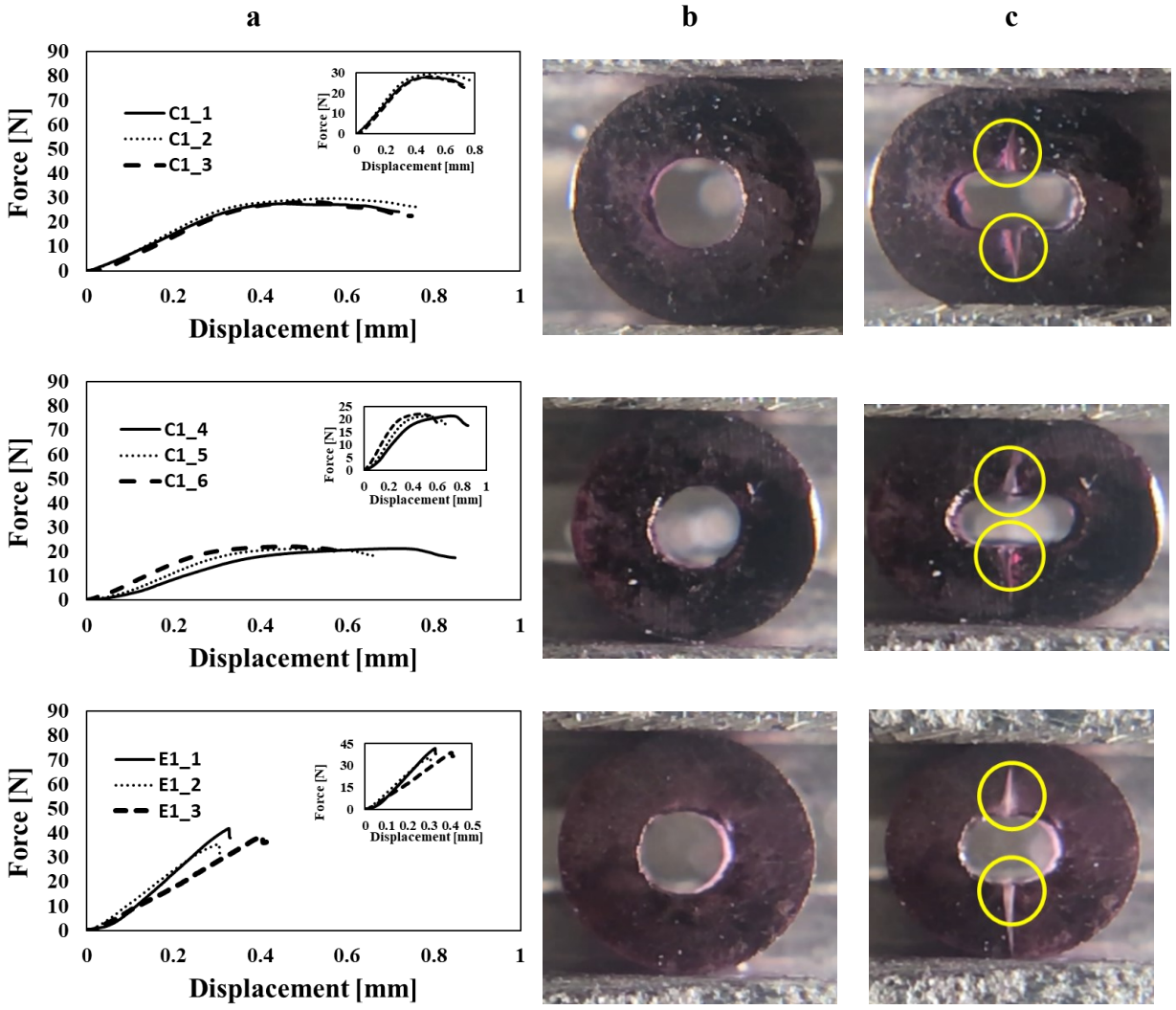

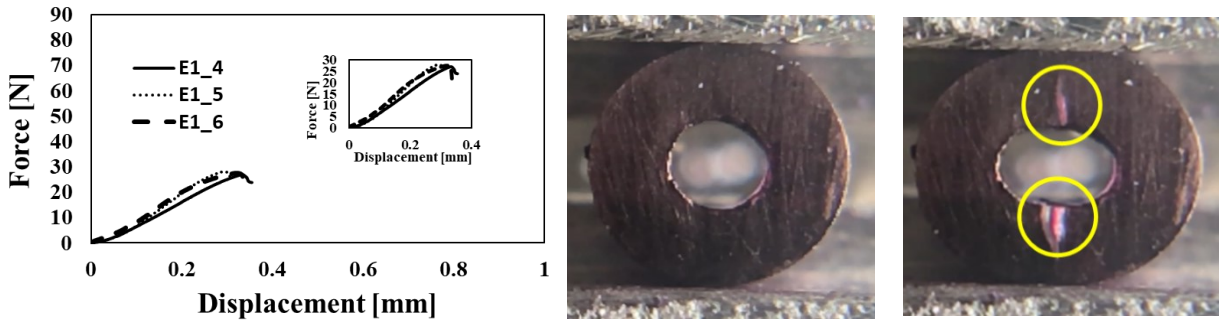

Fig. 5. (a) Force-displacement results obtained from the diametral compression test of the polymer adhesive ring specimens. Snapshots from the diametral compression test: (b) the undeformed specimen and (c) the specimen after failure (post-failure). Row 1: C1 adhesive at 1 mm/min loading rate. Row 2: C1 adhesive at 0.2 mm/min loading rate. Row 3: E1 adhesive at 1 mm/min loading rate. Row 4: E1 adhesive at 0.2 mm/min loading rate.

The post-failure pattern (Fig. 5(c)(Row 1)) of C1 adhesive ring specimen at the loading rate of 1 mm/min shows that the fracture initiated at the hole and propagated along the loading axis. In comparison, with the undeformed specimen (Fig. 5(b)(Row 1)), it is noted that the failure evolves towards the contact surfaces with the load platens. Additionally, C1 adhesive specimen appears highly deformed by compression while reaching failure at 1 mm/min loading rate. In comparison, the shapes of the failed mineralized tissue specimens are similar to their undeformed shapes at both loading rates of 1 mm/min and 0.2 mm/min. This observation is complemented by the average failure displacement of C1 adhesive specimen at 1 mm/min loading rate that is larger than the average failure displacement of the mineralized tissue at both 1 mm/min and 0.2 mm/min loading rates.

C1 adhesive ring specimens that were subject to 0.2 mm/min loading rate resulted a peak force average of 21.56 N (Fig. 5(a)(Row 2)). The minimum peak force was 21.30 N and the maximum peak force was 22.06 N. The failure displacements were averaged as 0.55 mm where their minimum and maximum were 0.46 mm and 0.71 mm, respectively. For the C1 adhesive, the failure force at 0.2 mm/min loading rate is substantially lower than the failure force at 1mm/min

loading rate. On the other hand, C1 adhesive had almost the same average failure displacement at 0.2 mm/min as 1 mm/min loading rate. However, the minimum and maximum failure displacements at both loading rates suggests that C1 adhesive at 0.2 mm/min yields a relatively lower failure displacement than the failure displacement at 1 mm/min (see the Appendix, Table A2).

The experimental snapshots of C1 adhesive ring specimens at 0.2 mm/min loading rate show that the specimen started to fail at the hole along the load axis (Fig. 5(c)(Row 2)). Moreover, the orientation of the fracture path appears towards the loading surface by comparing the circled zone in (Fig. 5(c)(Row 2)) to the intact specimen in (Fig. 5(b)(Row 2)). The observed fracture pattern of C1 adhesive specimen at 0.2 mm/min is similar to its fracture pattern at 1 mm/min. C1 adhesive specimen underwent relatively higher deformation than the mineralized tissue at both loading rates of 1 mm/min and 0.2 mm/min before reaching the failure similar to its behavior at 1 mm/min loading rate.

The ring specimens made of E1 formulation resulted in the average peak force of 38.63 N at 1 mm/min loading rate (Fig. 5(a)(Row 3)). The lowest peak force of E1 specimens was 35.34 N and the highest peak force was 41.85 N. The displacement corresponding to the peak forces was averaged to be 0.34 mm where their minimum and maximum were 0.33 mm and 0.40 mm, respectively. At 1 mm/min loading rate, E1 adhesive specimens failed at a higher load compared to C1 adhesive and smaller load than the mineralized tissue. It is noted that the average failure displacement of E1 adhesive specimens at 1 mm/min closely approximated the average failure displacement of the mineralized tissue whereas it was smaller than C1 adhesive specimen's failure displacement at both 1 mm/min and 0.2 mm/min (see the Appendix, Table A2).

E1 adhesive ring specimens started failing along the loading axis (yellow circles) (Fig. 5(c)(Row 3)) at loading rate of 1 mm/min. When the intact specimen (Fig. 5(b)(Row 3)) is compared to the failed specimen (Fig. 5(c)(Row 3)), it is clear that the failure initiated at the hole and propagated to the load surface following the loading axis. The shape comparison of undeformed and failed E1 specimens indicates failure after relatively low deformation. Compared to C1 adhesive specimen at both loading rates, E1 adhesive specimens at 1 mm/min undergo much lower deformation before failure. The fracture path of E1 adhesive specimens is the same as both the mineralized tissue and C1 adhesive specimens at 1 mm/min and 0.2 mm/min loading rates.

When E1 adhesive ring specimens were subjected to 0.2 mm/min loading rate, the average peak force was 27.48 N (Fig. 5(a)(Row 4)). The minimum peak force was 26.95 N and the maximum was 28.05 N. The corresponding failure displacement resulted in an average of 0.32 mm with a minimum of 0.29 mm and a maximum of 0.33 mm. Compared with their behavior at 1 mm/min, E1 adhesive specimens failed at a lower load at 0.2 mm/min. However, the average failure force of E1 adhesive at 0.2 mm/min was quite close to C1 adhesive's average failure force at 1 mm/min. In terms of the average failure displacement, E1 adhesive was on the lower side compared to its average failure force at 1 mm/min and C1 adhesive's average failure force at both loading rates (see the Appendix, Table A2).

At the loading rate of 0.2 mm/min, fracture initiation was observed at the hole and it coincides with the loading axis (circled zone) as seen from Fig. 5(c)(Row 4). After the fracture initiates at the hole, it continues on the loading axis in the direction of the load platens. This fracture evolution is clearly seen by comparing the specimen before failure (Fig. 5(b)(Row 4)) and after failure (Fig. 5(c)(Row 4)). E1 adhesive specimen followed the same fracture pattern at 0.2 mm/min as its fracture pattern at 1 mm/min loading rate. Its post-failure shape was close to its undeformed

shape, as expected from the force-displacement relationship that indicates relatively low deformation while reaching the failure.

3.3 Interfacial Specimens

The interfacial specimens of the mineralized tissue – C1 adhesive had the average peak force of 86.67 N at 1 mm/min (Fig. 6(a)(Row 1)). Their lowest peak force was 70.75 N and the highest peak force was 93 N. Their failure displacements were averaged as 0.48 mm where the minimum and maximum were 0.38 mm and 0.62 mm, respectively. As expected, the mineralized tissue – C1 adhesive interfacial specimens failed at a higher load compared to mineralized tissue ring specimens at 1 mm/min loading rate. Besides, the failure displacement also increased with the inclusion of C1 adhesive in the specimen compared to the mineralized tissue ring specimen. However, the average failure displacement of the mineralized tissue – C1 adhesive interfacial specimens was smaller than C1 adhesive ring specimens' average failure displacement (see the Appendix, Table A2).

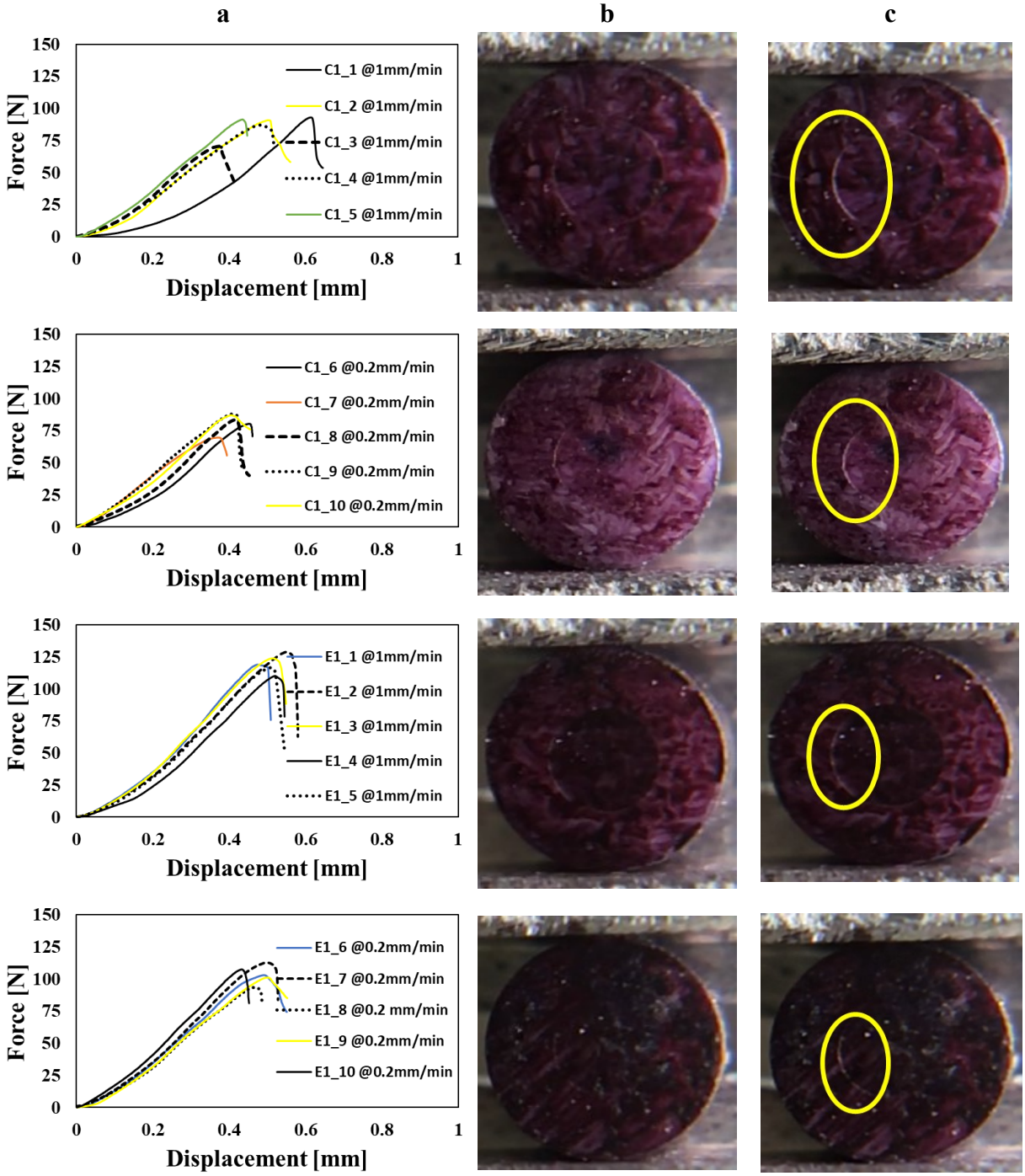

Fig. 6. (a) Force-displacement results obtained from the diametral compression test of the interfacial specimens. Snapshots from the diametral compression test: (b) the undeformed specimen and (c) the specimen after failure (post-failure). Row 1: the mineralized tissue – C1 adhesive at 1 mm/min loading rate. Row 2: the mineralized tissue – C1 adhesive at 0.2 mm/min

loading rate. Row 3: the mineralized tissue – E1 adhesive at 1 mm/min loading rate. Row 4: the mineralized tissue – E1 adhesive at 0.2 mm/min loading rate.

As seen from Fig. 6(b)(Row 1) and Fig. 6(c)(Row 1), there is a discoloration zone at the interface on the transverse axis to the loading axis on the surface of the failed specimen (yellow circle, Fig. 6(c)(Row 1)). When this discoloration zone is compared to the intact specimen (Fig. 6(b)(Row 1)), it is observed that the failure evolves at the interface orthogonal to the loading axis. This fracture pattern of the mineralized tissue – C1 adhesive interfacial specimen was quite different from both the mineralized tissue and adhesive specimens. For both the mineralized tissue and adhesive specimens, the fracture pattern was inside out from the hole along the load axis.

When interfacial specimens made of mineralized tissue and C1 adhesive were tested at 0.2 mm/min loading rate, the average peak force was 81.69 N with a minimum of 69.70 N and a maximum of 88.07 N (Fig. 6(a)(Row 2)). When the specimens reached their peak forces, they resulted in the displacement average as 0.41 mm. The minimum failure displacement was 0.37 mm whereas the maximum was 0.45 mm. It is clearly seen that the mineralized tissue – C1 adhesive interfacial specimens failed at both lower load and lower displacement at 0.2 mm/min than their average failure load and average failure displacement at 1 mm/min loading rate. It is also observed that the average failure force and failure displacement of the mineralized tissue – C1 adhesive specimens at 0.2 mm/min were higher than the mineralized tissue ring specimen's average failure force and displacement at 1 mm/min loading rate (see the Appendix, Table A2).

The experimental post-failure snapshot of the mineralized tissue – C1 interfacial specimen at 0.2 mm/min (Fig. 6(c)(Row 2)) shows the separation at the interface along the axis that is transverse to the loading axis (yellow circled). The interfacial separation gets smaller towards the

loading axis, indicating the propagation of the failure toward the load axis when the post-failure pattern is compared to the intact specimen (Fig. 6(b)(Row 2)). The post-failure pattern of the mineralized tissue – C1 adhesive interfacial specimen at 0.2 mm/min loading rate is the same as its post-failure pattern at 1 mm/min loading rate.

When the interfacial specimens made of the mineralized tissue and E1 adhesive were tested at 1 mm/min, they reached the average peak force of 119.72 N (Fig. 6(a)(Row 3)). The minimum peak force was 110.23 N and the maximum peak force was 129.16 N. The displacements corresponding to their peak forces were averaged as 0.51 mm where their lowest one was 0.48 mm and their highest one was 0.55 mm. The mineralized tissue – E1 adhesive interfacial specimens were significantly higher in the average failure load and displacement than the mineralized tissue – C1 adhesive interfacial specimens at 1 mm/min loading rate. They exhibited average failure displacement that is close to the average failure displacement of C1 adhesive ring specimens (see the Appendix, Table A2).

The failure initiation at the mineralized tissue – E1 adhesive interfacial specimen was observed at the interface on the transverse axis to the loading when the specimen was subject to the loading rate of 1 mm/min (Fig. 6(c)(Row 3)). The discoloration zone, which indicates the failure, appears to be smaller towards the load surfaces when the undeformed specimen (Fig. 6(b)(Row 3)) is compared with the failed interfacial specimen (Fig. 6(c)(Row 3)). This reveals that the fracture evolves toward the loading axis. Therefore, the fracture path of the mineralized tissue – E1 adhesive interfacial specimen at 1 mm/min loading rate was the same as the mineralized tissue – C1 adhesive interfacial specimen at both loading rates of 1 mm/min and 0.2 mm/min.

For the mineralized tissue – E1 adhesive interfacial specimens at 0.2 mm/min loading rate, the average failure load was 103.49 N with a minimum of 93.25 N and a maximum of 112.63 N

(Fig. 6(a)(Row 4)). They failed at an average displacement of 0.48 mm where the lowest failure displacement was 0.43 mm and the highest failure displacement was 0.50 mm. The mineralized tissue – E1 adhesive interfacial specimens reached failure at 0.2 mm/min loading rate at a lower load than their behavior at 1 mm/min loading rate whereas it was significantly higher than the average failure load of the mineralized tissue – C1 adhesive interfacial specimen's average failure load at 1 mm/min loading rate. Similarly, the average failure displacement of the mineralized tissue – E1 adhesive interfacial specimen at 0.2 mm/min was relatively lower than its average failure displacement at 1 mm/min loading rate. However, it was quite close to the average failure displacement of the mineralized tissue – C1 adhesive interfacial specimen at 1 mm/min (see the Appendix, Table A2).

When the snapshots of the diametral compression test on the interfacial specimen of the mineralized tissue – E1 adhesive are compared to the intact (Fig. 6(b)(Row 4)) and post-failure (Fig. 6(c)(Row 4)) states at 0.2 mm/min loading rate, it is observed that the specimen initiated failure at the interface along the transverse axis to the load axis. The propagation of the failure appeared in the direction towards the load axis along the interface. This failure pattern was the same as the mineralized tissue – E1 adhesive interfacial specimen at 1 mm/min loading rate and the mineralized tissue – C1 adhesive interfacial specimens at both 1 mm/min and 0.2 mm/min loading rates (see the Appendix, Table A2).

4. Discussion

It is noted that all force-displacement relationships obtained from both the ring specimens and the interfacial specimens experienced a small concave upward trend in the measurement. This type of behavior is likely due to the stiffening associated with the growing area between the surface of the specimen and the load platens [37]. As it is seen from the force-displacement curves, the

hardening mechanism competes with the softening mechanism. Initially, the hardening mechanism is dominant and the specimens' response gets stiffer at each load increment. However, the softening mechanism, most likely caused by accumulation of the damage within the specimen, takes over close to the yielding observed in the force-displacement curve. In materials that experience dissipation due to combination of damage and rate dependency it is empirically not possible to identify the dominant source of softening at a particular loading stage (see for example [55]). As the damage increases, the specimens reach failure and eventually, they experience post-peak softening.

When the post-failure snapshots of specimens are compared to the intact shape of the specimens, it is noted that the failure pattern is the same for all ring specimens. The failure is initiated as a discoloration at hole that coincides with the diametral load axis. Afterward, the failure propagates along the diametral axis towards the loading surface while the discoloration intensifies. Eventually, the specimen experiences abrupt fracture when the specimen cannot resist more separation along the diametral axis.

On the other hand, the interfacial specimens exhibit a different failure pattern than the failure pattern of ring specimens, although they have the same failure pattern when compared to each other. The failure of the interfacial specimens starts at the interface that coincides with the transverse axis to the diametral load axis. It is noted that this failure or separation at the interface is observed only on one side of the interface. This behavior likely results from the randomly heterogeneous defect distribution in the mineralized tissue section of the interfacial specimens. This heterogeneity might cause discontinuities in the stress distribution, such as stress concentrations that will likely lead to the asymmetrical failure pattern at the interface. Besides, the asymmetrical failure pattern might arise from the variation in the uniformity of bonding at the

interface. The bonding uniformity at the interface will be thoroughly examined via Raman spectroscopy in the future. Moreover, it is also seen that the failure propagates along the interface towards the intersection of the interface with the diametral load axis. This particular failure path can be attributed to the mineralized tissue section. It is already noted that the specimen fails at the hole along the loading axis when there is no inclusion in the ring specimens. In the presence of the inclusion, the initial failure is shifted towards the transverse axis and grows towards the loading axis along the interface. The failure evolves along the interface and later propagates to the mineralized tissue along the loading axis. Notably, this failure shift location was observed to be the failure initiation location of the mineralized tissue ring specimens [37]. It may be possible that the mineralized tissue starts accumulating damage at this location when the failure initiates at the interface. Therefore, the failure shift location can be considered as a secondary failure location.

The ring specimens were prepared to include a preset weakness to promote and control the initial failure location. It also complements the understanding of the failure of the interfacial specimens since the identical mineralized tissue ring specimens were used to prepare the interfacial specimens. The results from the diametral compression test of the mineralized tissue ring specimens were compared to published data. Comprehensive results were available for the mechanical strength of human cortical bone [56]. The published data was reported in terms of stress. To enable one to one comparison, the force measurements in this study were converted into stress. To this end, the apparent tensile strength of the ring specimen was calculated by using the following equation [57-60]:

$$\sigma_t = 2P(6 + 38\bar{r}^2)/\pi Dt \qquad \textbf{(Eq. 1)}$$

where σ_t is the apparent tensile strength of a ring specimen, P is the measured force, $\bar{r}$ is the ratio of the hole diameter to the outer diameter, D is the outer diameter and t is the thickness of the

specimen. The average apparent tensile strength of the mineralized tissue specimens was 112.23 MPa and 74.47 MPa at 1 mm/min and 0.2 mm/min loading rates, respectively. The apparent tensile strength calculated using (Eq. 1) is in the range of the tensile strength reported in the literature for human cortical bone [56]. It is noted, however, that the literature values (1) often do not report the loading rates or use rates that are different from that used in this work, and (2) have a much wider variation likely due to the natural variability of the tissue and also the uncertainty of the testing procedure [56].

The data obtained from the testing of the polymer adhesives were also calculated in terms of their apparent tensile strength. The average tensile strength of C1 and E1 adhesives at 1 mm/min loading rate was calculated as 35.11 MPa and 43.91 MPa, respectively. Moreover, C1 and E1 adhesives have an apparent tensile strength of 26.56 MPa and 31.24 MPa, respectively, at 0.2 mm/min loading rate.

Similarly, the data obtained from the testing of the interfacial specimens were converted into apparent tensile strength by using the following equation [33, 57, 61, 62]:

$$\sigma_t = 2P/\pi Dt \qquad \textbf{(Eq. 2)}$$

where σ_t is the apparent tensile strength of a disk specimen, P is the measured force, D is the disk diameter and t is the disk thickness. It is noteworthy that Eq. 2 applies only to the center of a homogeneous disc and is used here only to provide an estimate of the bond strength. For the bond strength characterization, it was assumed that the apparent tensile strength is the bond strength since it was observed that the interfacial specimens reached failure at the interface. To this end, the average bond strength data for the mineralized tissue – C1 adhesive interface was calculated as 12.26 MPa and 11.56 MPa at 1 mm/min and 0.2 mm/min loading rates, respectively. On the other hand, the mineralized tissue – E1 adhesive interface resulted in the average bond strength of

16.94 MPa and 14.64 MPa at loading rates of 1 mm/min and 0.2 mm/min, respectively, which are comparable to published data from conventional bond strength characterization of dentin-adhesive interface via micro-tensile test [26, 27] and a diametral compression test on dentin-adhesive-composite interface for bond strength characterization [34]. In detail, a recent study followed a similar approach using the diametral compression test on interfacial specimens where the specimens were prepared as three sections [34]. These three sections were bovine dentin tissue as the mineralized tissue at the outer section, a bonding agent as adhesive in the middle section and restorative composite at the inclusion section. Moreover, the specimens in that study were tested in a vertical configuration whereas in this study the specimens were tested in a horizontal configuration. The testing configuration can potentially affect the application of the assumed boundary conditions due to the alignment of the specimen during loading. Both vertical and horizontal configurations are considered applicable to this measurement. In particular, the horizontal configuration improves the alignment between the load platens. The improved alignment of a specimen establishes convenience in the application of desired boundary conditions for the diametral compression test. While considering these differences, it is noted that the results from the published investigation provide a benchmark to verify the reliability of the bond strength characterization in this study.

Furthermore, the higher loading rate yielded higher average failure force and displacement for all materials and interfacial pairs. This observation is due to the viscoelastic nature of both the mineralized tissue and the polymer adhesive materials where the viscoelastic material stiffens with the increasing loading rate (see the Appendix, Table A2).

When C1 and E1 adhesives are compared in terms of their failure load at both 1 mm/min and 0.2 mm/min loading rates, it is seen that E1 adhesive's failure load is higher than C1 adhesive at

both loading rates. This finding can be explained by the mechanical response of amorphous polymer that is strongly affected by the crosslinking density [63]. E1 adhesive polymer has higher crosslinking density due to the further contribution of the sol-gel reaction to strengthen the polymer network [44-46]. However, the higher crosslinking density is also why E1 adhesive specimens failed at a lower displacement compared to the C1 adhesive specimens. This phenomenon is suggested by a molecular dynamics simulation study where more strain concentrations emerged from a higher crosslinking density [63]. Eventually, the specimen fails in a more brittle manner with the increased strain concentrations, which is observed by comparing brittle failure of E1 adhesive, whose crosslinking density is higher than C1 adhesive that failed in a more ductile manner. Moreover, at the higher loading rate E1 adhesive showed a significant increase in failure load as compared to the C1 adhesive (see the Appendix, Table A2). This behavior of E1 adhesive may be due to the relaxation of pedant side chains and dynamic hydrogen bonds where the increasing loading rate requires a shorter process for dissociation of reversible cross-links [64]. The effects of cross-linking on failure and rate-dependence through changes in elastic modulus as well as viscous dissipation need further investigation informed by theories and relationships that are both representative and robust [65].

In the bond strength measurement, it is observed that the mineralized tissue – E1 adhesive interface yields significantly higher bond strength than the mineralized tissue – C1 adhesive interface at both 1 mm/min and 0.2 mm/min loading rates (see the Appendix, Table A2). This superior mechanical strength of the mineralized tissue – E1 adhesive can be addressed by the hydrolyzed MPS in E1 adhesive. The hydrolyzed MPS contains three silanol groups whereas C1 adhesive has no silanol groups and has less amount of hydrogen bond donor/acceptor [48]. A condensation reaction between the silanol and hydroxyl groups of collagen could lead to additional

bonding. This will reduce the polymer/collagen chain mobility and inhibit the plastic flow while being deformed. Moreover, the theoretical density of polymer and polymer/collagen hybrid materials is determined by the crosslinker content. The chain reorganization possibility diminishes with higher crosslinking density [66, 67] and this is reflected in higher stiffness [68, 69]. The hybrid networks also stiffen since the motion of the side chain can be hindered by more hydrogen bonds such as silanol-silanol, silanol-hydroxyl and silanol-collagen, etc.) [70].

5. Summary and Conclusions

The dental restorative materials design lacks a reliable measurement of mechanical properties. To address this limitation, we investigated the mechanical properties of the bovine cortical bone tissue – dental adhesive interface and its components experimentally. Due to compositional similarities and accessibility, the bovine cortical bone tissue was preferred as a surrogate material for human dentin. The diametral compression test was performed to reveal the tensile nature of the mineralized tissue (the cortical bone) and the adhesive polymers, as well as the bond strength of the mineralized tissue – adhesive interface. Two different adhesive formulations were investigated during this study, i.e. the experimental formulation contained γ-methacryloxypropyl trimethoxysilane (MPS) while the control (C1) formulation did not. MPS was reported to provide self-strengthening characteristics to the adhesives.

After performing the tests at two different loading rates, the tensile strength of the materials and the bond strength of the interfacial material systems were evaluated. The rate-dependent nature was distinctly observed for the mineralized tissue, adhesive polymers and the interfacial material systems. Both the tensile strength of the bovine cortical bone tissue and the bond strength of the mineralized tissue – adhesive interface were found to be in good agreement with the literature. The experimental post-failure snapshots revealed failure initiation locations and paths of failure

evolution in both single material and interfacial testing. The self-strengthening adhesive, E1, had higher tensile strength and bond strength to the mineralized tissue as compared to C1 adhesive. Under tensile loading, the self-strengthening adhesive, E1, is brittle in comparison to C1 adhesive. (see the Appendix, Table A2). The difference in the mechanical behavior was mainly linked to the properties of E1 adhesive. These properties include a higher crosslinking density, more hydrogen bonds and lower chain mobility than C1 adhesive. It is noted that the mechanical test technique selected in this study effectively eliminated the drawbacks inherent to the conventional tensile testing. However, the physical experiment alone may not necessarily deliver the true mechanics underlying the tensile nature and bond mechanics [37] as well as the granular nature of both the mineralized tissue and the cross-linked adhesive polymer [71-73]. A deeper understanding of the true tensile nature and bonding characteristics of these material systems can be established through the assistance of complementary techniques such as finite element analysis and digital image correlation to reveal stress and strain distribution on the domain of interest, such as hybrid layer, where the deformation and failure mechanisms can be investigated thoroughly. Future work will consider predictive models closely with the experimental data to obtain the distribution and evolution of stresses and strains during the loading process to understand the mechanism of failure initiation and propagation, including the prediction of fracture toughness.

Acknowledgements

This research was supported by the research grants CMMI-1727433 from the National Science Foundation (AM) and R01DE025476 (PS, CT, AM) from the National Institute of Dental and Craniofacial Research, National Institutes of Health, Bethesda, Maryland.

Author contributions

AM, PS and CT together conceived the experimental program presented in this work. RS performed the experiments and analyzed the data. QY and LS developed the adhesive formulations and assisted in the development of the sample preparation protocols. All authors collaborated in data interpretation, discussion and the writing of the manuscript.

Appendix

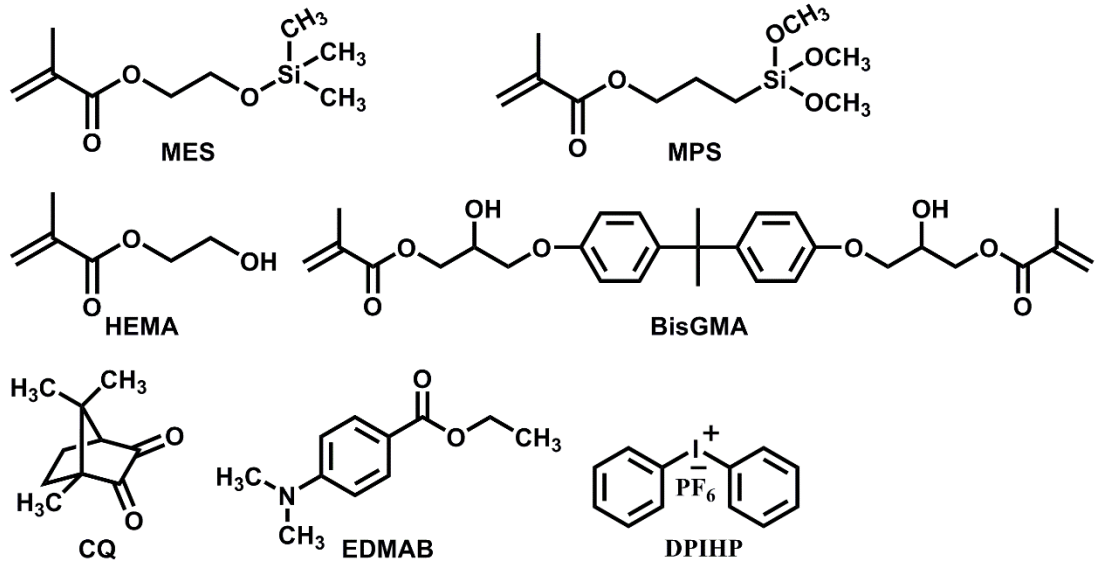

Fig. A1. Chemical structures of components that were used in the formulations [48].

Table A1. Composition of C1 and E1 formulations. (C1: Control and E1: Experimental)

Run (wt%)	C1	E1
HEMA	58	58
BisGMA	30	30
MES	10	-
MPS	-	10
CQ	0.5	0.5
EDMAB	0.5	0.5
DPIHP	1.0	1.0
Total	100	100

The following table presents the mean, the minimum and the maximum failure force and failure displacement values obtained from the diametral compression tests.

Table A2. The failure force and failure displacement results obtained in the experiments. The results are presented in the mean, minimum and maximum values for all specimens at all loading rates.

		Peak force [N]			Peak displacement [mm]		
Specimen	**Load rate [mm/min]**	**Mean**	**Min**	**Max**	**Mean**	**Min**	**Max**
Mineralized tissue	1	77.61	69.49	84.11	0.39	0.37	0.44
	0.2	51.50	48.90	56.44	0.28	0.27	0.31
C1 polymer	1	28.50	27.57	29.74	0.52	0.46	0.57
	0.2	21.56	21.30	22.06	0.55	0.46	0.71
E1 polymer	1	38.63	35.34	41.85	0.34	0.33	0.40
	0.2	27.48	26.95	28.05	0.32	0.29	0.33
Mineralized tissue - C1 interface	1	86.67	70.75	93.00	0.48	0.38	0.62
	0.2	81.69	69.70	88.07	0.41	0.37	0.45
Mineralized tissue - E1 interface	1	119.72	110.23	129.16	0.51	0.48	0.55
	0.2	103.49	93.25	112.63	0.48	0.43	0.50

References

[1] D.H. Pashley, F.R. Tay, L. Breschi, L. Tjaderhane, R.M. Carvalho, M. Carrilho, A. Tezvergil-Mutluay, State of the art etch-and-rinse adhesives, Dental Materials 27(1) (2011) 1-16.
[2] P. Kalesinskas, T. Kacergius, A. Ambrozaitis, V. Peciuliene, D. Ericson, Reducing dental plaque formation and caries development. A review of current methods and implications for novel pharmaceuticals, Stomatologija 16(2) (2014) 44-52.

[3] L. Tjaderhane, F.D. Nascimento, L. Breschi, A. Mazzoni, I.L.S. Tersariol, S. Geraldeli, A. Tezvergil-Mutluay, M. Carrilho, R.M. Carvalho, F.R. Tay, D.H. Pashley, Strategies to prevent hydrolytic degradation of the hybrid layer-A review, Dental Materials 29(10) (2013) 999-1011.
[4] L. Breschi, A. Mazzoni, A. Ruggeri, M. Cadenaro, R. Di Lenarda, E.D. Dorigo, Dental adhesion review: Aging and stability of the bonded interface, Dental Materials 24(1) (2008) 90-101.
[5] R.S. Schwartz, R. Fransman, Adhesive dentistry and endodontics: Materials, clinical strategies and procedures for restoration of access cavities: A review, Journal of Endodontics 31(3) (2005) 151-165.
[6] J. De Munck, K. Van Landuyt, M. Peumans, A. Poitevin, P. Lambrechts, M. Braem, B. Van Meerbeek, A critical review of the durability of adhesion to tooth tissue: Methods and results, Journal of Dental Research 84(2) (2005) 118-132.
[7] G.B.D.O.D. Collaborators, E. Bernabe, W. Marcenes, C.R. Hernandez, J. Bailey, L.G. Abreu, V. Alipour, S. Amini, J. Arabloo, Z. Arefi, A. Arora, M.A. Ayanore, T.W. Barnighausen, A. Bijani, D.Y. Cho, D.T. Chu, C.S. Crowe, G.T. Demoz, D.G. Demsie, Z.S. Dibaji Forooshani, M. Du, M. El Tantawi, F. Fischer, M.O. Folayan, N.D. Futran, Y.C.D. Geramo, A. Haj-Mirzaian, N. Hariyani, A. Hasanzadeh, S. Hassanipour, S.I. Hay, M.K. Hole, S. Hostiuc, M.D. Ilic, S.L. James, R. Kalhor, L. Kemmer, M. Keramati, Y.S. Khader, S. Kisa, A. Kisa, A. Koyanagi, R. Lalloo, Q. Le Nguyen, S.D. London, N.D. Manohar, B.B. Massenburg, M.R. Mathur, H.G. Meles, T. Mestrovic, A. Mohammadian-Hafshejani, R. Mohammadpourhodki, A.H. Mokdad, S.D. Morrison, J. Nazari, T.H. Nguyen, C.T. Nguyen, M.R. Nixon, T.O. Olagunju, K. Pakshir, M. Pathak, N. Rabiee, A. Rafiei, K. Ramezanzadeh, M.J. Rios-Blancas, E.M. Roro, S. Sabour, A.M. Samy, M. Sawhney, F. Schwendicke, F. Shaahmadi, M.A. Shaikh, C. Stein, M.R. Tovani-Palone, B.X. Tran, B. Unnikrishnan, G.T. Vu, A. Vukovic, T.S.S. Warouw, Z. Zaidi, Z.J. Zhang, N.J. Kassebaum, Global, Regional, and National Levels and Trends in Burden of Oral Conditions from 1990 to 2017: A Systematic Analysis for the Global Burden of Disease 2017 Study, J Dent Res 99(4) (2020) 362-373.
[8] R. Sarikaya, L. Song, E. Yuca, S.-X. Xie, K. Boone, A. Misra, P. Spencer, C. Tamerler, Bio-inspired multifunctional adhesive system for next generation bio-addivitely designed dental restorations, Journal of the Mechanical Behavior of Biomedical Materials 113 (2020) 104135.
[9] P. Spencer, Q. Ye, L.Y. Song, R. Parthasarathy, K. Boone, A. Misra, C. Tamerler, Threats to adhesive/dentin interfacial integrity and next generation bio-enabled multifunctional adhesives, Journal of Biomedical Materials Research Part B-Applied Biomaterials 107(8) (2019) 2673-2683.
[10] X. Zhou, X. Huang, M. Li, X. Peng, S. Wang, X. Zhou, L. Cheng, Development and status of resin composite as dental restorative materials, Journal of Applied Polymer Science 136(44) (2019) 48180.
[11] C.A. Stewart, Y. Finer, Biostable, antidegradative and antimicrobial restorative systems based on host-biomaterials and microbial interactions, Dental Materials 35(1) (2019) 36-52.
[12] A. Misra, P. Spencer, O. Marangos, Y. Wang, J.L. Katz, Parametric study of the effect of phase anisotropy on the micromechanical behaviour of dentin-adhesive interfaces, J R Soc Interface 2(3) (2005) 145-57.
[13] V. Singh, A. Misra, O. Marangos, J. Park, Q. Ye, S.L. Kieweg, P. Spencer, Fatigue life prediction of dentin-adhesive interface using micromechanical stress analysis, Dent Mater 27(9) (2011) e187-95.

[14] P. Spencer, Q. Ye, J. Park, E.M. Topp, A. Misra, O. Marangos, Y. Wang, B.S. Bohaty, V. Singh, F. Sene, J. Eslick, K. Camarda, J.L. Katz, Adhesive/Dentin interface: the weak link in the composite restoration, Ann Biomed Eng 38(6) (2010) 1989-2003.
[15] J.P. Matinlinna, L.V. Lassila, I. Kangasniemi, A. Yli-Urpo, P.K. Vallittu, Shear bond strength of Bis-GMA resin and methacrylated dendrimer resins on silanized titanium substrate, Dent Mater 21(3) (2005) 287-96.
[16] P.E. Cardoso, R.R. Braga, M.R. Carrilho, Evaluation of micro-tensile, shear and tensile tests determining the bond strength of three adhesive systems, Dent Mater 14(6) (1998) 394-8.
[17] N. Kanemura, H. Sano, J. Tagami, Tensile bond strength to and SEM evaluation of ground and intact enamel surfaces, J Dent 27(7) (1999) 523-30.
[18] S.R. Armstrong, D.B. Boyer, J.C. Keller, Microtensile bond strength testing and failure analysis of two dentin adhesives, Dent Mater 14(1) (1998) 44-50.
[19] J.M. Patierno, F.A. Rueggeberg, R.W. Anderson, R.N. Weller, D.H. Pashley, Push-out strength and SEM evaluation of resin composite bonded to internal cervical dentin, Endod Dent Traumatol 12(5) (1996) 227-36.
[20] L. De Lorenzis, A. Rizzo, A. La Tegola, A modified pull-out test for bond of near-surface mounted FRP rods in concrete, Composites Part B-Engineering 33(8) (2002) 589-603.
[21] Y. Shimada, S. Yamaguchi, J. Tagami, Micro-shear bond strength of dual-cured resin cement to glass ceramics, Dental Materials 18(5) (2002) 380-388.
[22] A. Hashimoto, H. Ohno, M. Kaga, H. Sano, F.R. Tay, H. Oguchi, Y. Araki, M. Kubota, Over-etching effects on micro-tensile bond strength and failure patterns for two dentin bonding systems, Journal of Dentistry 30(2-3) (2002) 99-105.
[23] S. Armstrong, S. Geraldeli, R. Maia, L.H. Raposo, C.J. Soares, J. Yamagawa, Adhesion to tooth structure: a critical review of "micro" bond strength test methods, Dent Mater 26(2) (2010) e50-62.
[24] S.S. Scherrer, P.F. Cesar, M.V. Swain, Direct comparison of the bond strength results of the different test methods: a critical literature review, Dent Mater 26(2) (2010) e78-93.
[25] S. Phrukkanon, M.F. Burrow, M.J. Tyas, Effect of cross-sectional surface area on bond strengths between resin and dentin, Dent Mater 14(2) (1998) 120-8.
[26] J.L. Ferracane, J.M. Dossett, F. Pelogia, M.R. Macedo, T.J. Hilton, Navigating the dentin bond strength testing highway: lessons and recommendations, Journal of adhesion science and technology 23(7-8) (2009) 1007-1022.
[27] P. Spencer, A. Misra, Material-tissue Interfacial Phenomena: Contributions from Dental and Craniofacial Reconstructions, Woodhead Publishing2016.
[28] B. Ramanathan, V. Raman, Split tensile strength of cohesive soils, Soils and Foundations 14(1) (1974) 71-76.
[29] Standard Test Method for Splitting Tensile Strength of Intact Rock Core Specimens, ASTM International, 2016.
[30] Standard Test Method for Splitting Tensile Strength of Cylindrical Concrete Specimens, ASTM International, 2004.
[31] P. Jonsen, H.A. Haggblad, K. Sommer, Tensile strength and fracture energy of pressed metal powder by diametral compression test, Powder Technology 176(2-3) (2007) 148-155.
[32] C. Shang, I.C. Sinka, J. Pan, Modelling of the break force of tablets under diametrical compression, International Journal of Pharmaceutics 445(1-2) (2013) 99-107.
[33] D. Zaytsev, P. Panfilov, Deformation behavior of human enamel under diametral compression, Materials Letters 136 (2014) 130-132.

[34] C.A. Carrera, Y.-C. Chen, Y. Li, J. Rudney, C. Aparicio, A. Fok, Dentin-composite bond strength measurement using the Brazilian disk test, Journal of dentistry 52 (2016) 37-44.
[35] S.-H. Huang, L.-S. Lin, J. Rudney, R. Jones, C. Aparicio, C.-P. Lin, A. Fok, A novel dentin bond strength measurement technique using a composite disk in diametral compression, Acta biomaterialia 8(4) (2012) 1597-1602.
[36] L. Zhu, Y. Li, Y.-C. Chen, C.A. Carrera, C. Wu, A. Fok, Comparison between two post-dentin bond strength measurement methods, Scientific reports 8(1) (2018) 1-8.
[37] A. Misra, R. Sarikaya, Computational analysis of tensile damage and failure of mineralized tissue assisted with experimental observations, Proceedings of the Institution of Mechanical Engineers, Part H: Journal of Engineering in Medicine (2019) 0954411919870650.
[38] H. Sano, T. Yoshikawa, P. Pereira, N. Kanemura, M. Morigamui, J. Tagami, D.H. Pashley, Long-term durability of dentin bonds made with a self-etching primer, in vivo, Journal of dental research 78(4) (1999) 906-911.
[39] M.J. Soappman, A. Nazari, J.A. Porter, D. Arola, A comparison of fatigue crack growth in resin composite, dentin and the interface, dental materials 23(5) (2007) 608-614.
[40] C.J. Kleverlaan, A.J. Feilzer, Polymerization shrinkage and contraction stress of dental resin composites, Dental Materials 21(12) (2005) 1150-1157.
[41] J.-F. Roulet, Benefits and disadvantages of tooth-coloured alternatives to amalgam, Journal of dentistry 25(6) (1997) 459-473.
[42] P. Spencer, Q.Y.J. PARK, A. Misra, B.S. Bohaty, V. Singh, R. Parthasarathy, F. Sene, S.E. de Paiva GONÇALVES, J. Laurence, Durable bonds at the adhesive/dentin interface: an impossible mission or simply a moving target?, Brazilian dental science 15(1) (2012) 4.
[43] J. Kruzic, R. Ritchie, Fatigue of mineralized tissues: cortical bone and dentin, Journal of the mechanical behavior of biomedical materials 1(1) (2008) 3-17.
[44] S.-X. Xie, K. Boone, S.K. VanOosten, E. Yuca, L. Song, X. Ge, Q. Ye, P. Spencer, C. Tamerler, Peptide Mediated Antimicrobial Dental Adhesive System, Applied Sciences 9(3) (2019) 557.
[45] L.Y. Song, Q. Ye, X.P. Ge, A. Misra, C. Tamerler, P. Spencer, Fabrication of hybrid crosslinked network with buffering capabilities and autonomous strengthening characteristics for dental adhesives, Acta Biomaterialia 67 (2018) 111-121.
[46] L.Y. Song, Q. Ye, X.P. Ge, A. Misra, P. spencer, Mimicking Nature: Self-strengthening Properties in a Dental Adhesive Acta Biomaterialia 35 (2016) 138-152.
[47] S.-X. Xie, L. Song, E. Yuca, K. Boone, R. Sarikaya, S.K. VanOosten, A. Misra, Q. Ye, P. Spencer, C. Tamerler, Antimicrobial Peptide–Polymer Conjugates for Dentistry, ACS Applied Polymer Materials 2(3) (2020) 1134-1144.
[48] R. Sarikaya, L. Song, Q. Ye, A. Misra, C. Tamerler, P. Spencer, Evolution of Network Structure and Mechanical Properties in Autonomous-Strengthening Dental Adhesive, Polymers (Basel) 12(9) (2020).
[49] Y.M. Chen, T.F. Xi, Y.F. Zheng, L. Zhou, Y.Z. Wan, In vitro structural changes of nano-bacterial cellulose immersed in phosphate buffer solution, Journal of Biomimetics, Biomaterials and Tissue Engineering, Trans Tech Publ, 2011, pp. 55-66.
[50] X. Guo, Y. Wang, P. Spencer, Q. Ye, X. Yao, Effects of water content and initiator composition on photopolymerization of a model BisGMA/HEMA resin, Dental Materials 24(6) (2008) 824-831.

[51] L. Song, Q. Ye, X. Ge, A. Misra, J.S. Laurence, C.L. Berrie, P. Spencer, Synthesis and evaluation of novel dental monomer with branched carboxyl acid group, Journal of Biomedical Materials Research Part B: Applied Biomaterials 102(7) (2014) 1473-1484.
[52] Q. Ye, J. Park, E. Topp, P. Spencer, Effect of photoinitiators on the in vitro performance of a dentin adhesive exposed to simulated oral environment, dental materials 25(4) (2009) 452-458.
[53] R. Parthasarathy, A. Misra, J. Park, Q. Ye, P. Spencer, Diffusion coefficients of water and leachables in methacrylate-based crosslinked polymers using absorption experiments, Journal of Materials Science: Materials in Medicine 23(5) (2012) 1157-1172.
[54] V. Singh, A. Misra, R. Parthasarathy, Q. Ye, P. Spencer, Viscoelastic properties of collagen–adhesive composites under water-saturated and dry conditions, Journal of Biomedical Materials Research Part A 103(2) (2015) 646-657.
[55] A. Misra, V. Singh, Thermomechanics-based nonlinear rate-dependent coupled damage-plasticity granular micromechanics model, Continuum Mechanics and Thermodynamics 27(4) (2015) 787-817.
[56] U. Wolfram, J. Schwiedrzik, Post-yield and failure properties of cortical bone, BoneKEy reports 5 (2016).
[57] R.A. Abdullah, T. Tsutsumi, Evaluation of tensile strength of Brazilian test under solid and ring disks using finite element analysis, Sains Malaysiana 47(4) (2018) 683-689.
[58] D. Hobbs, The tensile strength of rocks, International Journal of Rock Mechanics and Mining Sciences & Geomechanics Abstracts, Elsevier, 1964, pp. 385-396.
[59] J. Hudson, Tensile strength and the ring test, International Journal of Rock Mechanics and Mining Sciences & Geomechanics Abstracts, Elsevier, 1969, pp. 91-97.
[60] D.-y. Li, W. Tao, T.-j. Cheng, X.-l. Sun, Static and dynamic tensile failure characteristics of rock based on splitting test of circular ring, Transactions of Nonferrous Metals Society of China 26(7) (2016) 1912-1918.
[61] N. Erarslan, D.J. Williams, Experimental, numerical and analytical studies on tensile strength of rocks, International Journal of Rock Mechanics and Mining Sciences 49 (2012) 21-30.
[62] D. Li, L.N.Y. Wong, The Brazilian disc test for rock mechanics applications: review and new insights, Rock mechanics and rock engineering 46(2) (2013) 269-287.
[63] J.H. Zhao, P.S. Yu, S.H. Dong, The Influence of Crosslink Density on the Failure Behavior in Amorphous Polymers by Molecular Dynamics Simulations, Materials 9(4) (2016).
[64] J. Yang, C.Y. Shao, L. Meng, Strain Rate-Dependent Viscoelasticity and Fracture Mechanics of Cellulose Nanofibril Composite Hydrogels, Langmuir 35(32) (2019) 10542-10550.
[65] A. Misra, V. Singh, R. Parthasarathy, Material-tissue interfacial phenomena: challenges in mathematical modeling, Material-Tissue Interfacial Phenomena, Elsevier2017, pp. 253-264.
[66] I. Barszczewska-Rybarek, The role of molecular structure on impact resistance and bending strength of photocured urethane-dimethacrylate polymer networks, Polymer Bulletin 74(10) (2017) 4023-4040.
[67] X.P. Ge, Q. Ye, L.Y. Song, P. Spencer, J.S. Laurence, Effect of crosslinking density of polymers and chemical structure of amine-containing monomers on the neutralization capacity of dentin adhesives, Dental Materials 31(10) (2015) 1245-1253.
[68] J.E. Elliott, L.G. Lovell, C.N. Bowman, Primary cyclization in the polymerization of bis-GMA and TEGDMA: a modeling approach to understanding the cure of dental resins, Dental Materials 17(3) (2001) 221-229.

[69] I.M. Barszczewska-Rybarek, Characterization of urethane-dimethacrylate derivatives as alternative monomers for the restorative composite matrix, Dental Materials 30(12) (2014) 1336-1344.
[70] J. Park, J. Eslick, Q. Ye, A. Misra, P. Spencer, The influence of chemical structure on the properties in methacrylate-based dentin adhesives, Dental Materials 27(11) (2011) 1086-1093.
[71] A. Misra, P. Poorsolhjouy, Granular micromechanics model for damage and plasticity of cementitious materials based upon thermomechanics, Mathematics and Mechanics of Solids 25(10) (2020) 1778-1803.
[72] A. Misra, V. Singh, Nonlinear granular micromechanics model for multi-axial rate-dependent behavior, International Journal of Solids and Structures 51(13) (2014) 2272-2282.
[73] D. Timofeev, E. Barchiesi, A. Misra, L. Placidi, Hemivariational continuum approach for granular solids with damage-induced anisotropy evolution, Mathematics and Mechanics of Solids (2020) 1081286520968149.